

Machine learning classification of fast radio bursts: I. supervised methods

Jia-Wei Luo^{1,2*}, Jia-Ming Zhu-Ge³ and Bing Zhang^{1,2}

¹*Nevada Center for Astrophysics, University of Nevada, Las Vegas, NV 89154, USA*

²*Department of Physics and Astronomy, University of Nevada, Las Vegas, NV 89154, USA*

³*Department of Astronomy, University of Science and Technology of China, Hefei 230026, China*

Accepted XXX. Received YYY; in original form ZZZ

ABSTRACT

Observationally, the mysterious fast radio bursts (FRBs) are classified as repeating ones and apparently non-repeating ones. While repeating FRBs cannot be classified into the non-repeating group, it is unknown whether the apparently non-repeating FRBs are actually repeating FRBs whose repetitions are yet to be discovered, or whether they belong to another physically distinct type from the repeating ones. In a series of two papers, we attempt to disentangle this mystery with machine learning methods. In this first paper, we focus on an array of supervised machine learning methods. We train the machine learning algorithms with a fraction of the observed FRBs in the first CHIME/FRB catalog, telling them which ones are apparently non-repeating and which ones are repeating. We then let the trained models predict the repetitiveness of the rest of the FRB data with the observed parameters, and we compare the predictions with the observed repetitiveness. We find that the models can predict most FRBs correctly, hinting towards distinct mechanisms behind repeating and non-repeating FRBs. We also find that the two most important distinguishing factors between non-repeating and repeating FRBs are brightness temperature and rest-frame frequency bandwidth. By applying the trained models back to the entire first CHIME catalog, we further identify some potentially repeating FRBs currently reported as non-repeating. We recommend a list of these bursts as targets for future observing campaigns to search for repeated bursts in a combination with the results presented in Paper II using unsupervised machine learning methods.

Key words: transients: fast radio bursts – methods: data analysis

1 INTRODUCTION

Fast radio bursts (FRBs) are a type of millisecond luminous cosmic bursts in the radio wavelength (Lorimer et al. 2007; Thornton et al. 2013; Petroff et al. 2022; Cordes & Chatterjee 2019) whose origins have yet been brought to light (Platts et al. 2019; Zhang 2020; Xiao et al. 2022). Many models on the origin of FRBs have been proposed, albeit not a single one of them is able to explain all FRB phenomena (for reviews, see e.g. Katz 2016; Platts et al. 2019; Zhang 2020; Xiao et al. 2022).

While most FRBs are observed as one-off events, a small fraction, the first of which is FRB 20121102 (Spitler et al. 2016), show repeated bursts with a range of bursting rates. These repeating FRBs eliminated the possibility of cataclysmic event models being applied to all FRBs. However, an argument can still be made that repeating and non-repeating FRBs originate from different progenitors, and that only repeating FRBs rise from repeatable mechanisms (for discussions, see e.g. Katz 2022).

Prior to testing which physical model can explain the properties of the two potential types of FRBs, the existence of such dichotomy must first be proved (Palaniswamy et al. 2018; Ravi 2019; Caleb et al. 2019; Lu et al. 2020; Ai et al. 2021; Guo & Wei 2022; Zhong et al. 2022). There are some studies on the differences between repeating and non-repeating FRBs, pointing out some difference in parameter distributions of repeating and non-repeating FRBs such as burst width, bandwidth, spectral shape, energy and brightness temperature (Andersen et al. 2019; Fonseca et al. 2020; Li et al. 2021a; Aggarwal 2021; CHIME/FRB Collaboration et al. 2021; Pleunis et al. 2021; Li et al. 2021b; Xiao & Dai 2022; Zhang et al. 2022; Cui et al. 2022). However, these comparisons usually only consider differences within a single set of parameters, and cannot uncover discrepancies in combination of parameters in a higher dimensional parameter space.

A way to mitigate this limitation is through machine learning. Machine learning algorithms can analyze a large amount of data simultaneously and are capable of highlighting patterns in very high-dimensional data with minimal human intervention (for reviews on the application of machine learn-

* luoj7@unlv.nevada.edu

ing in astronomy, see e.g. [Ball & Brunner 2012](#); [Baron 2019](#); [Ivezić et al. 2014](#)).

There are two main approaches of machine learning: supervised and unsupervised. Supervised machine learning algorithms are used to learn a mapping from a set of input features to a set of labels, with the latter being inputted by human experts. After training, supervised machine learning algorithms can automatically label new input data without human input. Unsupervised machine learning algorithms, on the other hand, only take features as input and do not take labels. The unsupervised machine learning algorithm only knows the appearance of the data, but does not know which class each data point belongs to. It attempts to group input data points that looked similar into different clusters, without knowing or explaining the physical relationship of the clusters.

While machine learning methods are already widely used in aiding discovery of FRBs (see e.g. [Wagstaff et al. 2016](#); [Zhang et al. 2018](#); [Connor & van Leeuwen 2018](#); [The CHIME/FRB Collaboration 2019](#); [Wu et al. 2019](#); [Farah et al. 2019](#); [Adámek & Armour 2020](#); [Agarwal et al. 2020](#); [Yang et al. 2021](#)), few studies have employed machine learning methods to the classification of previously discovered FRBs, especially with supervised machine learning methods. [Chen et al. \(2021\)](#) used unsupervised machine learning methods to find apparent non-repeating FRBs that share similar observed parameters with the apparent repeating ones, and identified some repeater candidates. [Chaikova et al. \(2022\)](#), on the other hand, found two clusters of FRBs with distinct properties with similar unsupervised machine learning methods.

Supervised machine learning differs from unsupervised methods used by above-mentioned studies in that the supervised algorithms are able to make deterministic predictions of individual FRBs instead of clusters of FRBs, and can thus be more useful in identifying repeater candidates.

In this paper, we utilize a wide array of supervised machine learning algorithms implemented in `scikit-learn` ([Pedregosa et al. 2011](#)) and other open-source libraries and apply them to the classification of repeating and non-repeating FRBs. In Section 2, we describe the input data and features we utilize and construct. In Section 3, we introduce the data pre-processing procedure and model evaluation methods. In Section 4, we report the machine learning models and the outputs from them. We also compare the prediction accuracy of different models, as well as the importance of different observational parameters to the binary classification of repeating and non-repeating FRBs. In Section 5, we apply the trained models back to the entire dataset and attempt to uncover hidden repeating FRBs. In Section 6, we draw our conclusions. In a companion paper ([Zhu-Ge et al. 2022](#)), we conduct a set of unsupervised machine learning methods to classify the same data set. The consistency between the two methods is checked and the overlapping repeating FRB candidates are reported in Table 1.

2 DATA

We use the first CHIME/FRB catalog ([CHIME/FRB Collaboration et al. 2021](#)), which has a total of 536 FRBs observed between July 25, 2018 and July 1, 2019. Among them are 474 non-repeating bursts, and 62 bursts from 18 repeat-

ing FRB sources. We treat each sub-burst as an independent burst, and we exclude 6 bursts without flux measurements (FRB20190307A, FRB20190307B, FRB20190329B, FRB20190329C, FRB20190531A, FRB20190531B, all non-repeating). This leaves us with 594 individual bursts including sub-bursts, consisting of 500 bursts from the apparently non-repeating category and 94 bursts from the repeating category.

The input features to the machine learning algorithms in this study can be classified into two types: primary features that are drawn directly from the CHIME catalog, and secondary features that are calculated from primary features.

The distributions of the input features are shown in Fig. 1, with the details discussed below:

2.1 Primary features

- Box-car width (s)

This width represents a rough measure of the duration of the entire burst combining all sub-bursts ([CHIME/FRB Collaboration et al. 2021](#), the same below). The CHIME catalog also provides a more sophisticated `fitburst` width, which we utilize to calculate rest widths later in this section.

- Flux (Jy)

The flux reported by the CHIME catalog is the peak flux averaged across the frequency band. For bursts with sub-bursts, the CHIME catalog provides one single flux and we adopt the same value for all of the sub-bursts.

- Fluence (Jy ms)

The Fluence reported by the CHIME catalog is the integral of the flux time series across the burst extent and averaged across the frequency band. This value is also the same for sub-bursts in a burst as provided by the CHIME catalog.

- Excess dispersion measure (pc cm^{-3})

Excess dispersion measure (DM) is the DM of the FRB excluding the galaxy disk component. We use the NE2001 electron-density model ([Cordes & Lazio 2003](#)) values provided by the CHIME collaboration. This value is the same for sub-bursts.

- Peak frequency (MHz)

Peak frequency is the frequency corresponding to the highest flux density. This value is different for different sub-bursts.

The CHIME catalog provides scattering time as a representation of scattering of an FRB, but due to the degeneracy with the intrinsic shape of the burst, this parameter is given as an upper limit if the confidence level is not high enough from the CHIME FRB fitting routine `fitburst` ([CHIME/FRB Collaboration et al. 2021](#); [Chawla et al. 2022](#)). It is not straightforward to incorporate upper limits together with other values for machine learning algorithms, so we do not use scattering time in this study.

The CHIME catalog also provides spectral information of FRBs as spectral index and spectral running fitted with a powerlaw with running model ([CHIME/FRB Collaboration et al. 2021](#); [Chawla et al. 2022](#)). We found this universal model difficult to apply as some FRBs are fitted with spectral indices of ~ 50 . Thus we do not include these two features in our model. The spectral properties of FRBs are represented by peak frequency and frequency bandwidth.

2.2 Secondary features

- Redshift

In the CHIME 1st catalog, only two sources have measured redshifts through localization. In these two cases, we adopt their true redshifts: FRB20121102A at $z = 0.19273$ and FRB20180916B at $z = 0.0337$ (Tendulkar et al. 2017; Marcote et al. 2020).

For the majority of bursts without directly measured redshifts, we use the observed DMs to estimate z following the standard procedure. In general, the observed DM of an FRB can be broken down into four components (e. g. Thornton et al. 2013; Deng & Zhang 2014; Prochaska & Zheng 2019):

$$\text{DM} = \text{DM}_{\text{MW}} + \text{DM}_{\text{Halo}} + \text{DM}_{\text{IGM}} + \frac{\text{DM}_{\text{Host}}}{1+z}, \quad (1)$$

where DM_{MW} is the contribution from the Milky way disk, DM_{Halo} is the contribution from the Milky way halo, DM_{IGM} is the contribution from inter-galactic medium (IGM), and DM_{Host} is the contribution from the FRB host galaxy. The observed host galaxy DM is decreased by a factor of $(1+z)$ due to cosmological effects.

Among these four components, DM_{IGM} is directly tied to the redshift of the FRB through (Deng & Zhang 2014; Gao et al. 2014; Zhou et al. 2014; Macquart et al. 2020; Li et al. 2020; Cui et al. 2022, see also Ioka (2003); Inoue (2004)):

$$\text{DM}_{\text{IGM}}(z) = \frac{3cH_0\Omega_b f_{\text{IGM}}}{8\pi Gm_p} \int_0^z \frac{\chi(z)(1+z)}{\sqrt{\Omega_m(1+z)^3 + \Omega_\Lambda}} dz \quad (2)$$

Where c is the speed of light, G is the gravitational constant, $\chi(z)$ is a factor denoting ionized electrons to baryons in the IGM, which $\sim 7/8$ if both H and He are fully ionized, m_p is the mass of protons, and f_{IGM} is the fraction of baryons in the IGM. We assume χ to be a constant of $7/8$, and $f_{\text{IGM}} \sim 0.83$ (Fukugita et al. 1998; Li et al. 2020) and adopt the cosmology parameters measured by Planck (Aghanim et al. 2020): $H_0 = 67.4 \text{ km s}^{-1} \text{ Mpc}^{-1}$, $\Omega_m = 0.315$, $\Omega_b = 0.0493$ and $\Omega_\Lambda = 0.685$.

To obtain DM_{IGM} , one must first deduct the other components from the observed DM. For DM_{MW} we use the NE2001 electron-density model (Cordes & Lazio 2003). We assume DM_{Halo} to be a constant of 30 pc cm^{-3} , and $\text{DM}_{\text{Host}} = 70 \text{ pc cm}^{-3}$ following other studies (Xu & Han 2015; Dolag et al. 2015; Shannon et al. 2018; Li et al. 2020; Yamasaki & Totani 2020; Hashimoto et al. 2020; Arcus et al. 2021). Then, by considering the $1+z$ factor in the observed host galaxy DM, the redshift of the FRBs can be solved numerically with SciPy (Virtanen et al. 2020). We acknowledge that there is a large uncertainty in estimating z but nonetheless adopt the solution as the best estimate of the z value of a particular burst. We also set a minimum redshift of 0.00225, corresponding to a luminosity distance of 10 Mpc to avoid zero or negative values.

With redshift, we can derive several other features (as discussed below). We do not directly include redshift in our models. Rather, redshift is incorporated indirectly through other features.

- Brightness temperature (K)

For an FRB with peak specific flux S_ν , duration Δt and observed central frequency ν , and redshift z , the full expression

of brightness temperature should be:

$$\begin{aligned} T_B &= \frac{S_\nu D_A^2}{2\pi k_B (\nu \Delta t)^2} (1+z)^3 = \frac{S_\nu D_L^2}{2\pi k_B (\nu \Delta t)^2 (1+z)} \\ &= 1.1 \times 10^{35} \text{ K} \left(\frac{S_\nu}{\text{Jy}} \right) \left(\frac{\nu}{\text{GHz}} \right)^{-2} \left(\frac{\Delta t}{\text{ms}} \right)^{-2} \left(\frac{D_A}{\text{Gpc}} \right)^2 (1+z)^3 \\ &= 1.1 \times 10^{35} \text{ K} \left(\frac{S_\nu}{\text{Jy}} \right) \left(\frac{\nu}{\text{GHz}} \right)^{-2} \left(\frac{\Delta t}{\text{ms}} \right)^{-2} \left(\frac{D_L}{\text{Gpc}} \right)^2 \frac{1}{1+z}. \end{aligned} \quad (3)$$

where k_B is Boltzmann constant, D_A is the angular diameter distance of the FRB, D_L is the luminosity distance of the FRB.

This expression differs from the previously suggested expression involving the angular distance D_A (Zhang 2020; Xiao et al. 2021; Xiao & Dai 2022) by including a $(1+z)^3$ correction factor to account for cosmological effects. For a flat universe, the luminosity distance is connected with the angular distance via $D_L = D_A(1+z)^2$ (Etherington 1933; Ellis 2007), so T_B can be also calculated with D_L with a $(1+z)^{-1}$ correction factor. There are two independent ways of deriving Equation (3) in a self-consistent way, which are presented in Appendix A.

- Rest-frame width (s)

The rest-frame width is calculated by correcting the time-dilation effect, i.e.

$$\Delta t_r = \frac{\Delta t}{1+z}, \quad (4)$$

where Δt is the observed sub-burst width given by `fitburst`. This value is fitted with an FRB profile model and is different for different sub-bursts in the same burst.

- Rest-frame frequency bandwidth (MHz)

$$\Delta \nu = (\nu_{\text{max}} - \nu_{\text{min}})(1+z) \quad (5)$$

where ν_{max} and ν_{min} are the highest and lowest observed frequencies of the burst reported in the CHIME catalog in units of MHz.

- Burst energy (erg)

We follow Zhang (2018); Zhang et al. (2021); Li et al. (2021a); Hashimoto et al. (2022) to calculate the burst energy:

$$E = 4\pi D_L^2 F \nu_c / (1+z) \quad (6)$$

Where F is the fluence of the FRB, and ν_c is peak frequency. Adopting ν_c rather than the bandwidth is more appropriate for wide-spectra FRBs such as the majority of the non-repeating ones (Zhang 2018). It overestimates the energy of FRBs if the spectra have narrow bands. For consistency, we adopt ν_c for all the bursts since the majority of the bursts are apparently non-repeating ones.

3 METHODS

3.1 Pre-processing

We randomly split our data in a 7:3 ratio into a training set and a test set while keeping the original ratio of repeating to non-repeating FRBs in both sets. The former is used to train the machine learning algorithms, and the latter is used to test the performance of the machine learning models in

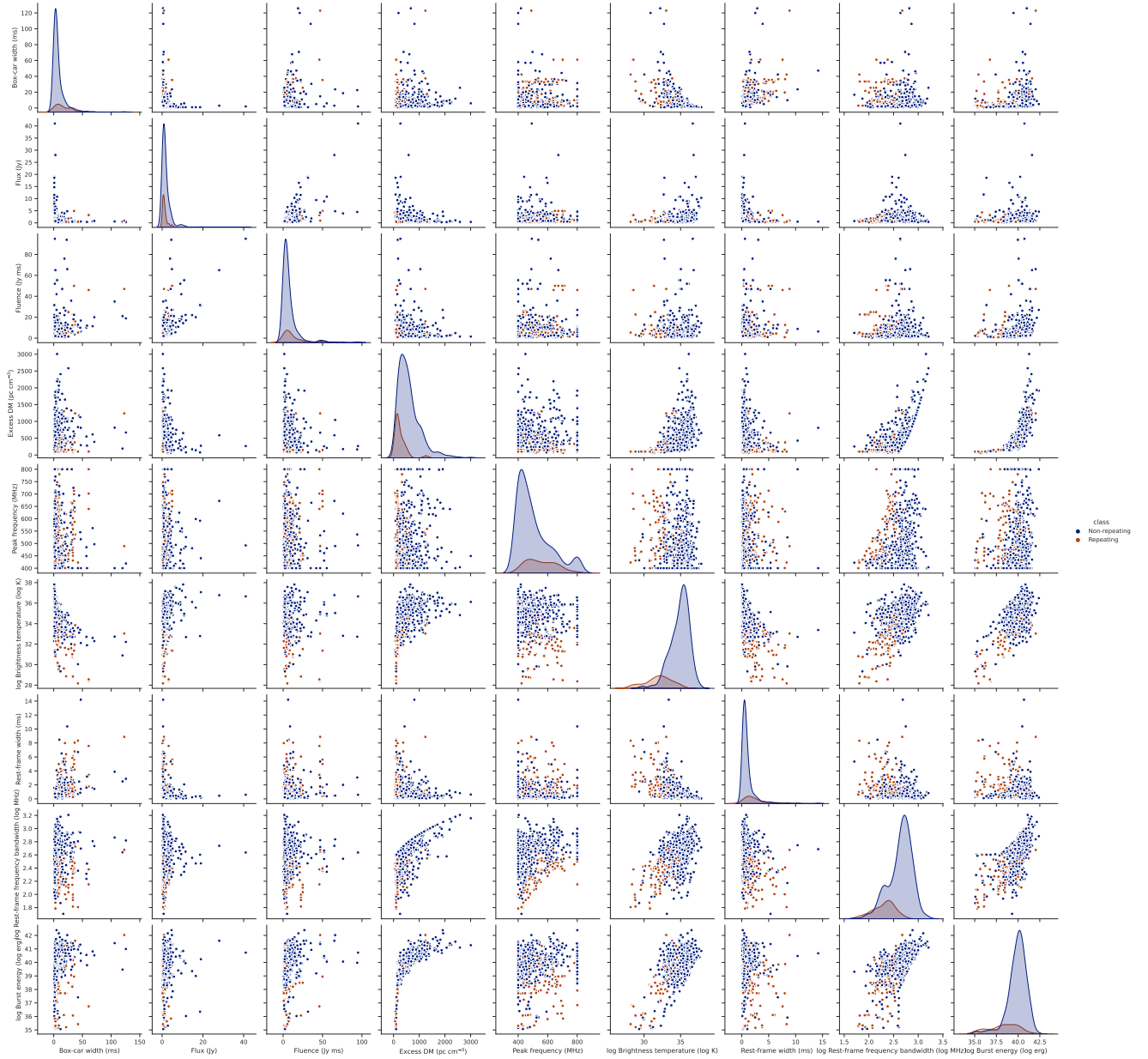


Figure 1. Corner plot of input feature distributions. The apparently non-repeating and repeating samples are denoted in blue and orange colors, respectively.

classifying the repeating and non-repeating FRBs. This split gives us 415 bursts (66 repeating and 349 non-repeating) in the training set and 179 bursts (28 repeating and 151 non-repeating) in the test set.

The input features have different ranges. The brightness temperature and burst energy are at orders $\sim 10^{30}$ and span across several orders of magnitude, while the box-car width and rest-frame width are at orders of $\sim 10^{-2}$. Hence, we need to normalize the input features. We first take the base 10 logarithms of brightness temperature, burst energy, and frequency bandwidth. We also convert the box-car width and rest-frame width to milliseconds. Then, we standardize the input features by removing the mean and scaling the variance

to unity. The standard distribution scaler is trained with the training set only, and subsequently applied to all the data.

The distribution of the two types of FRBs in our sample is significantly imbalanced. The size of the non-repeating FRB sample is $\sim 5\times$ that of the repeating FRBs. Because the true ratio of repeating to non-repeating FRBs is unknown, we need to avoid our models learning this apparent ratio. Therefore, we use the synthetic minority over-sampling technique (SMOTE) (Chawla et al. 2002) as implemented in `imbalanced-learn` (Lemaître et al. 2017) to over-sample the repeating FRB training set and make it the same size as the non-repeating FRB learning sample. Note that we only over-sample the training set, but keep the imbalance in the test set. This way we do not introduce any augmented data into the

testing process (Santos et al. 2018). After data augmentation, there are the same number of repeating and non-repeating FRBs in the training set (349).

3.2 Model evaluation

After training the models with the training set, we test the models with the test set. The most intuitive model evaluation metric is accuracy, defined as the ratio between the number of correctly predicted labels to the total number of input data points. However, this simple metric cannot be applied to our imbalanced data. Even a model simply predicts every FRB to be non-repeating can score 84.26% accuracy with our test set. Therefore, we need to find a more reliable method to evaluate our models.

There are two commonly used metrics in evaluating the performance of machine learning models, precision and recall:

- Precision

$$\text{Precision} = \frac{\text{True positives}}{\text{True positives} + \text{False positives}} \quad (7)$$

Precision measures how many of the items predicted by the model as positive (in this study repeating FRBs) are true positives.

- Recall

$$\text{Recall} = \frac{\text{True positives}}{\text{True positives} + \text{False negatives}} \quad (8)$$

Recall measures how many of the originally positive items are correctly predicted as positive by the model.

These two metrics are then usually combined to form the F_β score (van Rijsbergen 1979; Sasaki 2007):

$$F_\beta = (1 + \beta^2) \frac{\text{Precision} \cdot \text{Recall}}{(\beta^2 \cdot \text{Precision}) + \text{Recall}} \quad (9)$$

Where β is a weighting factor for precision and recall. The F_β score have a range of $0 \sim 1$, with $F_\beta = 1$ signaling a perfect model.

While it is common practice to let $\beta = 1$ and weight precision and recall equally, in this study precision and recall are not equal. An apparently non-repeating FRB could be a hidden repeating FRB yet to be seen repeating, but a repeating FRB cannot be a misidentified non-repeating one. A model that produces some false positives while yielding few false negatives should not be rejected. Therefore we let $\beta = 2$ to prioritize precision over recall. This way we can select models that find most apparent repeating FRB successfully, while retaining their ability to uncover possible hidden repeaters. We will refer to this metric as the F_2 score for the rest of the paper.

4 RESULTS

4.1 Simple decision tree method

Classification and Regression Trees (CART) is a type of simple machine learning algorithms where a decision tree of simple decision rules is created based on input features to predict corresponding labels or output values of new data (e.g. Breiman et al. 1984; Timofeev 2004; Loh 2011, 2014). In this

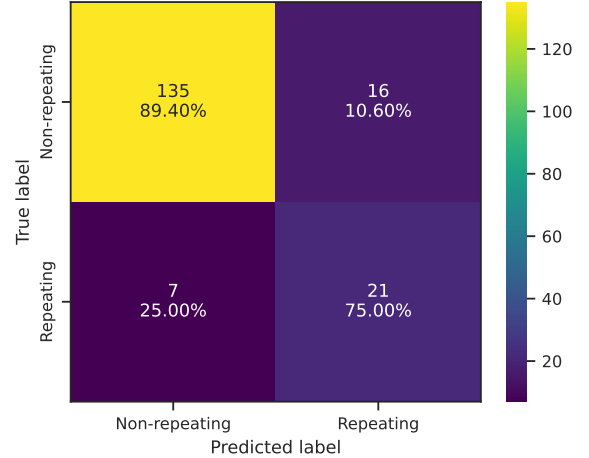


Figure 2. Confusion matrix of the decision tree method on the test set.

study, we build classification decision trees with the input features described in Section 2 and methods described in Section 3.

We found the default hyper-parameter settings of `scikit-learn` mostly work well for our problem, and altering the hyper-parameters does not really improve the results. Thus for the rest of this paper, we use default hyper-parameters unless otherwise stated.

We build a decision tree with a max depth of 5, and we are able to achieve a F_2 score of 0.7047. The decision path of this tree is shown in Figure 3.

We then build another decision tree with a max depth of 3, and only two input features: brightness temperature and rest-frame frequency bandwidth. We choose these two features because they are found to have the most feature importance later in this section. For this decision tree with 2 features, we are able to achieve $F_2 = 0.7759$. The confusion matrix is shown in Figure 4.

Figure 5 shows the log-log plot of brightness temperature and intrinsic frequency width. Most non-repeating FRBs reside in the top right corner, whereas most repeating FRBs reside in the lower left corner. While the repeating FRBs generally stay in their territory, many non-repeating FRBs permeate into the repeating region. This on one hand shows that the parameter distributions of repeating and non-repeating FRBs are significantly different, and on the other hand that some repeating FRBs are likely mis-classified as non-repeating.

4.2 Random forest method

For a single decision tree, it is difficult to balance bias and variance. If the depth is too shallow, then the decision tree will have difficulty in detecting all the positive items. On the other hand, if the depth is too deep, the decision tree will over-fit on the training data and perform badly on the test data.

To solve this problem, we employ the random forest algorithm (Breiman 2001). We randomly select sub-samples of the training set, and train many deep decision trees with

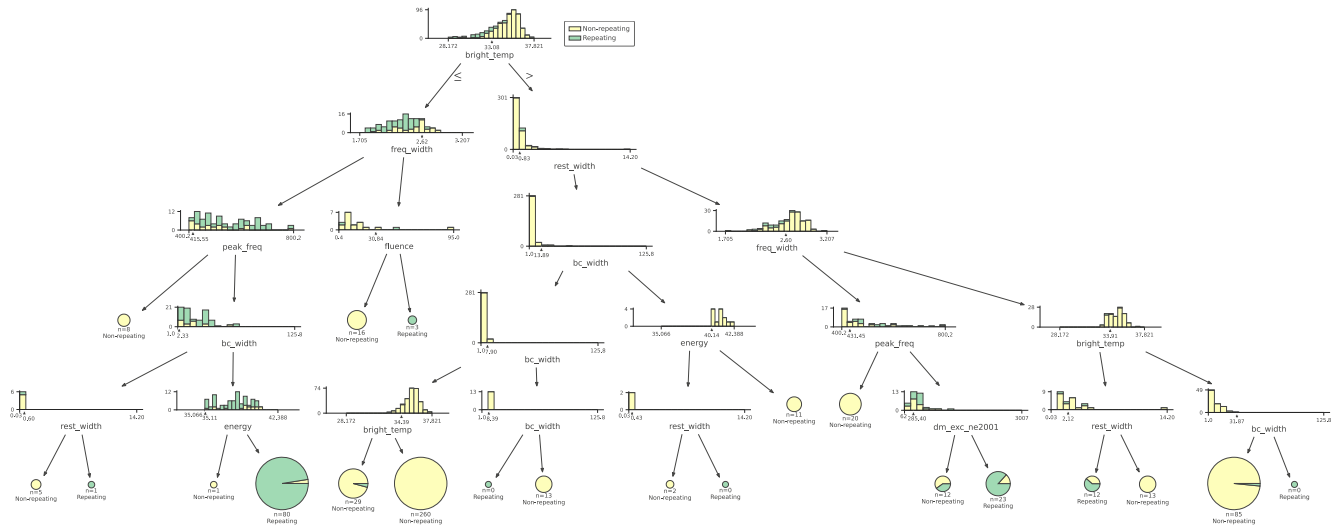


Figure 3. Decision paths of the decision tree on the entire dataset.

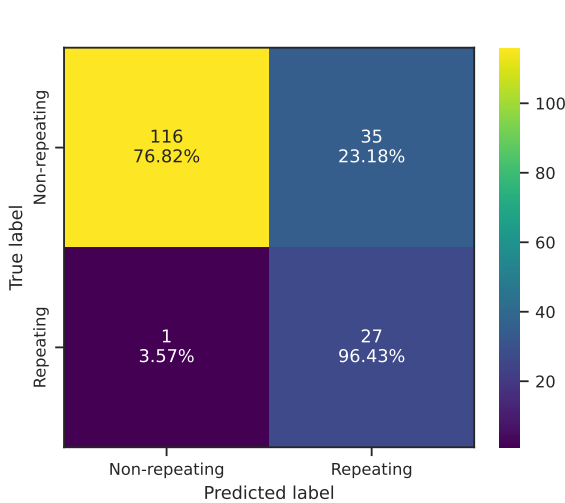


Figure 4. Confusion matrix of the decision tree with 2 features on the test set.

the random sub-samples that tend to over-fit. This process is called bagging (Breiman 1996). Then, the prediction of the ensemble of the deep decision trees is taken average to generate the output of the entire model to mitigate the over-fitting problem.

With this method, we are able to obtain an F_2 score of 0.8219. The confusion matrix is shown in Figure 6.

We also look into the importance of each input feature with permutation feature importance (Breiman 2001; Altmann et al. 2010; Fisher et al. 2019) on the entire dataset. Each time the values of one input feature are randomly shuffled across all data points, removing the correlation between this feature and the output label. The drop in model metric is observed to denote the importance of the feature. This process is repeated 100 times for each feature and the average from the trials are used as the final feature importance.

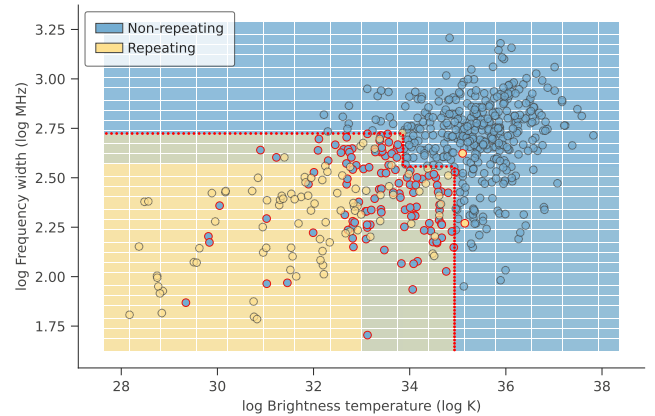


Figure 5. Decision boundary of the decision tree with 2 features on the entire dataset. The depth of colors represent the probability of either class.

The error bars are drawn with standard deviations from the trials.

The permutation feature importance for the random forest models is shown in Figure 7. Again, brightness temperature and rest-frame frequency bandwidth are of the highest importance to this model.

4.3 Boosted decision tree method

Another way to incorporate many decision trees into a single predictor is through boosting. In contrast to random forest, which uses deep decision trees trained on part of the data, boosting uses shallow decision trees trained on the entire data. The weak predictors are again taken average to obtain the final output (Freund & Schapire 1997; Drucker 1997; Friedman et al. 1998; Schapire & Singer 1999; Mayr et al. 2014).

There are different algorithm implementations of boosting. In this study, we employ AdaBoost (Freund & Schapire 1997),

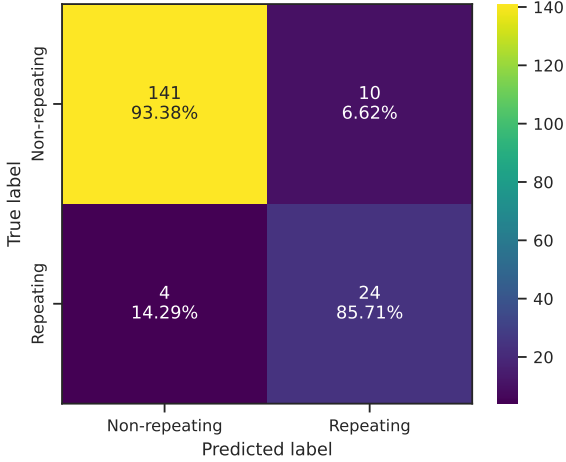


Figure 6. Confusion matrix of the random forest method on the test set.

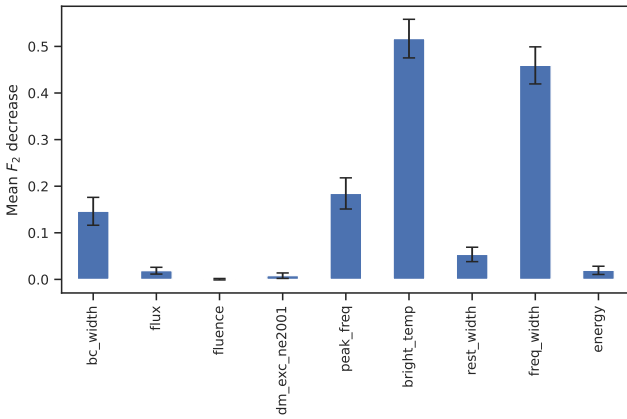


Figure 7. Permutation feature importance of the random forest method on the entire dataset.

LightGBM (Ke et al. 2017) and XGBoost (Chen & Guestrin 2016).

With AdaBoost, we obtain an F_2 score of 0.8725. We also get an F_2 score of 0.8503 and 0.8219 for LightGBM and XGBoost, respectively.

The confusion matrices and feature importance are shown in Figure 8 and Figure 9.

4.4 Support vector machine method

Support vector machine (SVM) (Cortes & Vapnik 1995) projects the input features onto a hyper-space, and then attempts to find a hyper-plane to separate the data points based on input labels. Since most inputs are not linearly separable, studies most commonly use the "kernel trick" (Hofmann et al. 2008) to project the data points to another coordinate to make them linearly separable.

We are able to achieve an F_2 score of 0.8125 with our

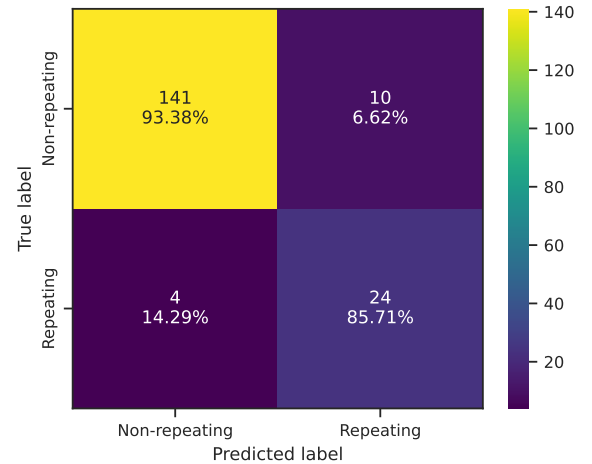
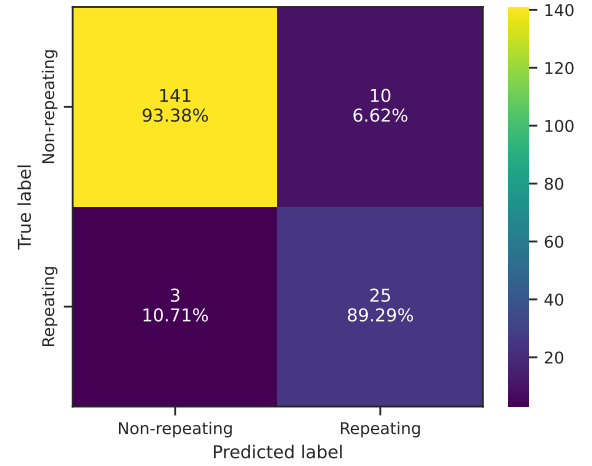
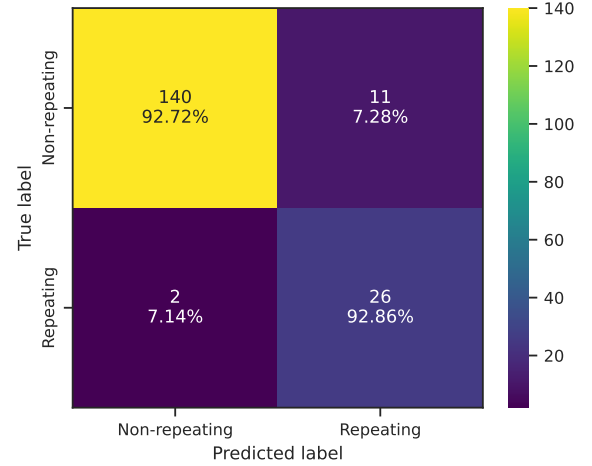


Figure 8. Confusion matrices for boosted decision tree methods on the test set. Upper: AdaBoost, middle: LightGBM, lower: XGBoost.

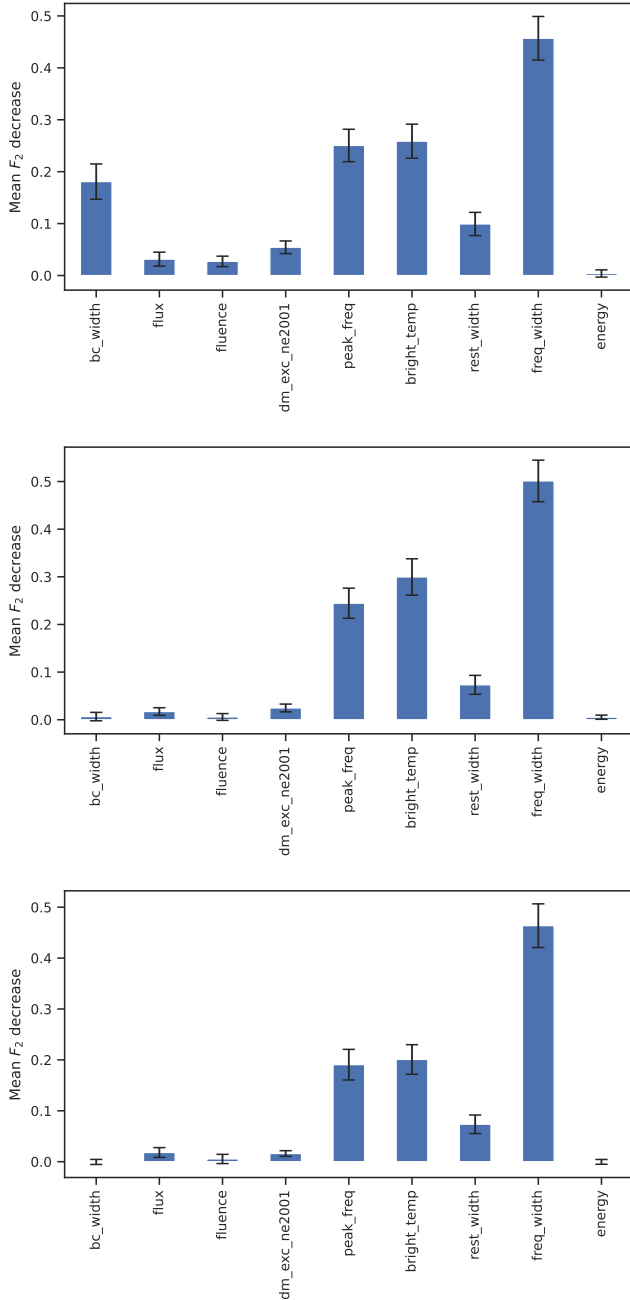


Figure 9. Permutation feature importance for boosted decision tree methods on the entire dataset. Upper: AdaBoost, middle: LightGBM, lower: XGBoost.

SVM model. The confusion matrix and feature importance are shown in Figure 10 and Figure 11.

4.5 Nearest centroid method

Similar to the SVM method, the nearest centroid method projects the data points into a hyperspace with their input features as position vectors (e.g. [Hastie et al. 2009](#)). The centroids of each class are learned by taking the average of the

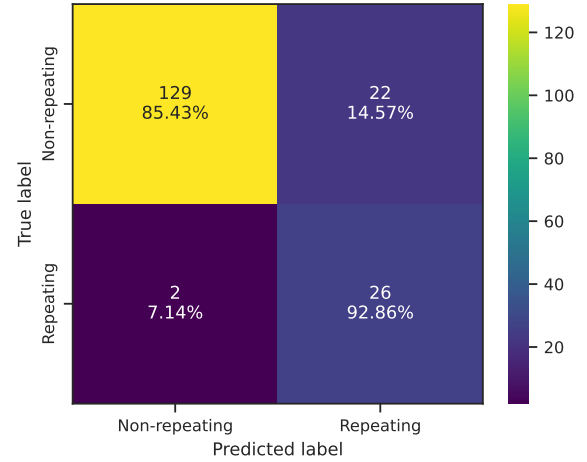


Figure 10. Confusion matrix for the SVM method on the test set.

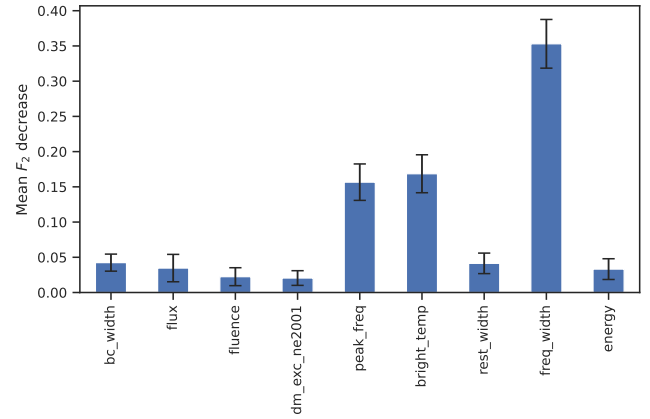


Figure 11. Permutation feature importance for the SVM method on the entire dataset.

positions of each class of the learning set. The predictions for the test set are determined by the nearest class centroid.

With this method, we can achieve an F_2 score of 0.8125. The confusion matrix and feature importance are shown in Figure 12 and Figure 13.

5 UNCOVERING HIDDEN REPEATING FRBS

5.1 Combining models

After training the models, we apply the models back to the entire CHIME catalog to find the bursts reported as non-repeating in the catalog but are predicted as repeating based on our machine learning models. Because the training-test set split introduces randomness to the results, we repeat the splitting and training process 1000 times. In each trial, if one apparently non-repeating bursts is predicted as repeating by at least 4 of the 6 models described in Section 4 except the simple decision tree method, we record this occurrence. We

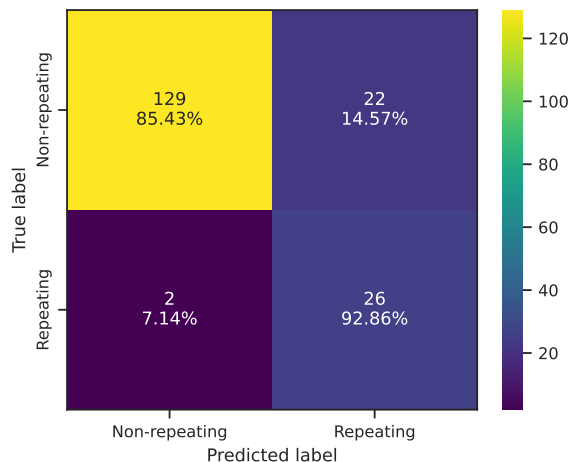


Figure 12. Confusion matrix for the nearest centroid method on the test set.

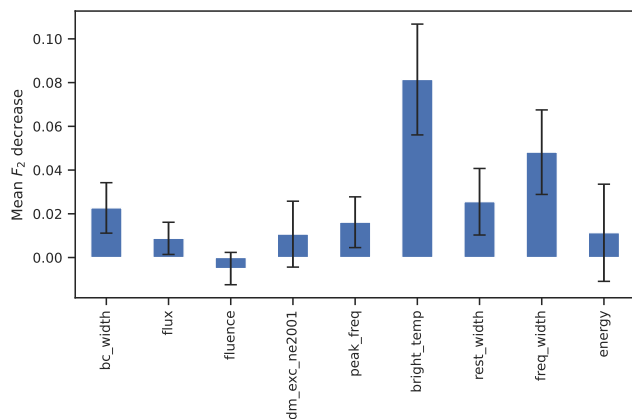


Figure 13. Permutation feature importance for the nearest centroid method.

further require that one burst needs to be predicted as a repeater in at least 100 trials to be identified as a repeater candidate.

The repeater candidates identified by this study, along with their input features and the number of trials predicted as repeating, are shown in Table 1.

5.2 Leave-one-out k -nearest neighbor

Another way to identify repeater candidates is Leave-one-out k -nearest neighbor. k -nearest neighbour (k -NN) classification (Fix & Hodges 1989; Altman 1992) takes the training set and project the feature vectors into a hyperspace. Then, for any prediction input, the model finds the nearest k training data points to the input feature vector. The prediction output label is then determined by the majority label of the nearest neighbors. In this study, we use $k = 5$.

In each cycle, one of the non-repeating burst is excluded from the training set, which consists of all the rest of the

data. Then, the one left out non-repeating burst is predicted with the trained model. If the output label is repeating, then this burst is identified as a repeater candidate. This method essentially looks at the “surrounding” bursts in the feature hyperparameter to determine if the left-out non-repeater is closer to the repeaters. The results are shown in Table 2.

5.3 Unsupervised learning and the strongest candidates

The classification results using unsupervised learning are reported in a companion paper (Zhu-Ge et al. 2022). Those methods also identified a list of repeater candidates which overlap with our predicted repeater candidates. In Table 1, we have highlighted the strongest candidates that are identified by all three methods, namely the combined supervised model, the leave-one-out KNN method and the unsupervised machine learning methods (enclosed in boxes). These candidates can be regarded as strong candidate targets for searching for repeated bursts.

6 CONCLUSIONS

In this paper, we have applied an array of supervised machine learning methods to the first CHIME FRB catalog, with the aim of categorizing repeating and non-repeating FRBs and identifying repeater candidates from the apparently non-repeating sample. We reach the following conclusions:

- The parameter distributions of repeating and non-repeating FRBs are significantly different from each other. Machine learning algorithms, even some simple ones, are able to distinguish them. The machine learning algorithms confirm the finding of the CHIME team (CHIME/FRB Collaboration et al. 2021) that spectral bandwidth is one key parameter to distinguish between the two categories. Furthermore, several algorithms identify brightness temperature (with a proper $(1+z)$ correction, see Eq.(3) and Appendix A) as another key parameter to distinguish the two categories.

- The fact that the machine learning algorithms can correctly predict the majority of the bursts hints that there likely exist two distinct types of FRBs. Most of the apparently non-repeating FRBs may either have a distinct type of central engine or a distinct radiation mechanism that is different from that of repeating FRBs.

- Some non-repeating FRBs are predicted as repeating FRBs by multiple models, suggesting they might be hidden repeaters yet to be uncovered. Many candidates are also identified from unsupervised machine learning methods reported in Paper II. We have identified several strong candidates by cross comparing the candidates from the two papers (Table 1) and recommend the community to search for repeated bursts from these sources. The algorithms applied in this paper can also be applied to newly discovered FRBs to predict whether they will repeat, which will help to arrange follow-up observations accordingly.

7 ACKNOWLEDGEMENTS

The authors thank Dongzi Li and Kiyoshi Masui for the information on the light curve and spectral parameters presented

Name	Sub Num	RA °	Dec °	Δt_{BC} ms	S_ν Jy	F_ν Jy ms	DM_E pc cm ⁻³	z	ν_c MHz	$\log T_B$ log K	Δt_r ms	$\log \Delta\nu$ log MHz	$\log E$ log erg	Score	Match
FRB20181229B	0	238.37	19.78	20.64	0.42	4.9	359.7	0.32	445.5	33.093	2.546	2.19	39.773	320	✓
FRB20190423B	0	298.58	26.19	9.83	0.87	7.0	102.3	0.003	537.6	29.813	2.482	2.204	35.931	316	✓+
FRB20190410A	0	263.47	-2.37	6.88	1.59	5.8	155.5	0.073	515.7	33.179	0.941	2.262	38.59	307	✓
FRB20181017B	0	237.76	78.5	12.78	1.06	6.5	263.7	0.207	593.2	33.271	1.914	2.394	39.628	301	✓+
FRB20181128C	0	268.77	49.71	14.75	0.39	3.4	569.2	0.557	480.3	33.785	1.477	2.42	40.144	301	
FRB20190422A	1	48.56	35.15	29.49	0.6	9.1	372.8	0.335	612.3	32.703	1.73	2.495	40.221	299	✓
FRB20190409B	0	126.65	63.47	30.47	0.39	6.8	237.8	0.175	545.5	32.008	1.991	2.528	39.464	296	✓
FRB20190329A	0	65.54	73.63	11.8	0.52	2.24	100.8	0.002	432.3	29.344	1.038	1.868	35.066	295	✓+
FRB20190423B	1	298.58	26.19	9.83	0.87	7.0	102.3	0.003	524.6	29.834	8.474	2.173	35.921	284	✓+
FRB20190206A	0	244.85	9.36	5.9	1.4	9.1	146.9	0.062	534.5	33.081	0.757	2.33	38.656	278	✓+
FRB20190128C	0	69.8	78.94	15.73	0.71	5.9	239.3	0.177	491.6	32.942	5.233	2.377	39.366	276	+
FRB20190106A	0	22.19	46.12	6.88	0.27	0.81	251.2	0.192	800.2	32.887	0.789	2.563	38.786	270	
FRB20190129A	0	45.06	21.42	8.85	0.49	5.0	432.7	0.404	707.7	33.703	0.805	2.541	40.191	270	✓
FRB20181030E	0	135.67	8.89	5.9	2.0	6.3	109.8	0.013	470.5	31.992	0.395	2.222	37.086	264	✓
FRB20190527A	0	12.45	7.99	57.02	0.47	10.1	550.9	0.537	484.7	32.651	1.737	2.313	40.588	261	✓+
FRB20190218B	0	268.7	17.93	17.69	0.57	5.9	466.3	0.442	588.0	33.409	1.422	2.524	40.264	259	✓
FRB20190609A	1	345.3	87.94	4.92	3.6	10.4	258.2	0.2	600.5	34.591	1.767	2.428	39.808	244	✓
FRB20190412B	0	285.65	19.25	42.27	0.68	12.8	110.9	0.015	400.2	30.045	6.702	2.359	37.416	239	✓+
FRB20190125B	0	231.45	50.54	6.88	0.83	4.7	145.0	0.059	609.9	32.57	2.332	2.627	38.391	239	+
FRB20181231B	0	128.77	55.99	2.95	0.89	2.34	150.3	0.066	657.7	33.366	0.316	2.442	38.217	229	✓+
FRB20181221A	0	230.58	25.86	4.92	1.25	5.8	291.8	0.24	510.1	34.438	0.608	2.231	39.648	187	✓
FRB20190112A	0	257.98	61.2	9.83	1.4	16.2	383.8	0.348	697.7	33.946	1.217	2.502	40.562	176	✓
FRB20190125A	0	45.73	27.81	13.76	0.37	2.6	504.3	0.484	655.5	33.428	2.162	2.634	40.038	174	
FRB20181218C	0	285.98	58.24	4.92	0.25	1.73	319.8	0.273	472.7	33.92	4.084	2.608	39.205	147	
FRB20190429B	0	329.93	3.96	16.71	0.74	5.0	253.5	0.194	422.4	33.122	5.342	1.705	39.311	138	✓+
FRB20190109B	0	253.47	1.25	6.88	1.2	3.0	106.9	0.009	408.1	31.455	0.337	1.969	36.397	137	✓+
FRB20190206B	0	49.76	79.5	19.66	0.95	9.6	274.0	0.219	506.4	33.039	5.824	2.544	39.78	126	

Table 1. List of repeater candidates from the combined models. Check mark ✓ indicates this FRB is also identified as a repeater candidate by Zhuge et al., plus mark + indicates this FRB is also identified as a repeater candidate by the leave-one-out k -NN method. The strongest candidates are marked with boxes around their names.

Name	Sub Num	RA °	Dec °	Δt_{BC} ms	S_ν Jy	F_ν Jy ms	DM_E pc cm ⁻³	z	ν_c MHz	$\log T_B$ log K	Δt_r ms	$\log \Delta\nu$ log MHz	$\log E$ log erg
FRB20180801A	0	322.53	72.72	9.83	1.11	7.9	565.6	0.553	595.6	34.399	0.373	2.32	40.597
FRB20180925A	0	74.93	77.99	14.75	0.99	8.7	167.1	0.088	800.2	32.093	4.156	2.602	39.12
FRB20180928A	0	312.95	30.85	2.95	1.34	2.5	94.7	0.002	400.2	31.027	0.268	1.963	35.08
FRB20181017B	0	237.76	78.5	12.78	1.06	6.5	263.7	0.207	593.2	33.271	1.914	2.313	39.628
FRB20181119B	0	299.38	31.12	22.61	4.5	94.0	166.8	0.087	536.4	32.723	3.063	2.602	39.976
FRB20181231B	0	128.77	55.99	2.95	0.89	2.34	150.3	0.066	657.7	33.366	0.316	2.414	38.217
FRB20190107A	0	0.86	21.81	47.19	0.49	6.3	809.3	0.824	400.2	33.377	14.198	2.426	40.678
FRB20190109B	0	253.47	1.25	6.88	1.2	3.0	106.9	0.009	408.1	31.455	0.337	1.965	36.397
FRB20190124E	0	297.75	20.57	18.68	0.64	7.3	225.8	0.161	625.6	32.451	4.945	2.602	39.476
FRB20190125B	0	231.45	50.54	6.88	0.83	4.7	145.0	0.059	609.9	32.57	2.332	2.602	38.391
FRB20190128C	0	69.8	78.94	15.73	0.71	5.9	239.3	0.177	491.6	32.942	5.233	2.307	39.366
FRB20190206A	0	244.85	9.36	5.9	1.4	9.1	146.9	0.062	534.5	33.081	0.757	2.304	38.656
FRB20190329A	0	65.54	73.63	11.8	0.52	2.24	100.8	0.002	432.3	29.344	1.038	1.867	35.066
FRB20190412B	0	285.65	19.25	42.27	0.68	12.8	110.9	0.015	400.2	30.045	6.702	2.353	37.416
FRB20190423B	0	298.58	26.19	9.83	0.87	7.0	102.3	0.003	537.6	29.813	2.482	2.202	35.931
FRB20190423B	1	298.58	26.19	9.83	0.87	7.0	102.3	0.003	524.6	29.834	8.474	2.172	35.921
FRB20190429B	0	329.93	3.96	16.71	0.74	5.0	253.5	0.194	422.4	33.122	5.342	1.627	39.311
FRB20190527A	0	12.45	7.99	57.02	0.47	10.1	550.9	0.537	484.7	32.651	1.737	2.126	40.588
FRB20190617B	0	56.43	1.16	13.76	0.99	9.2	229.7	0.166	459.3	33.201	6.504	2.271	39.469

Table 2. List of repeater candidates from leave-one-out KNN.

in the first CHIME FRB catalog, and the UNLV transient group members Shunke Ai, Connery Chen, Emily Huerta, and Yuanhong Qu, as well as Weiyang Wang for various discussions, especially on the derivations of FRB brightness temperature. Dian Shi is acknowledged for giving helpful advice on data pre-processing and machine learning model con-

structions. This work is partially supported by the Top Tier Doctoral Graduate Research Assistantship (TTDGRA) and Nevada Center for Astrophysics at the University of Nevada, Las Vegas.

DATA AVAILABILITY

The CHIME/FRB catalog used in this paper is public and is available at <https://www.chime-frb.ca/catalog>. The code can be shared upon request to the authors.

REFERENCES

- Adámek K., Armour W., 2020, *ApJS*, 247, 56
- Agarwal D., Aggarwal K., Burke-Spolaor S., Lorimer D. R., Garver-Daniels N., 2020, *MNRAS*, 497, 1661
- Aggarwal K., 2021, *ApJ*, 920, L18
- Aghanim N., et al., 2020, *A&A*, 641, A6
- Ai S., Gao H., Zhang B., 2021, *ApJ*, 906, L5
- Altman N. S., 1992, *The American Statistician*, 46, 175
- Altmann A., Tološi L., Sander O., Lengauer T., 2010, *Bioinformatics*, 26, 1340
- Andersen a. B. C., et al., 2019, *ApJ*, 885, L24
- Arcus W. R., Macquart J.-P., Sammons M. W., James C. W., Ekers R. D., 2021, *MNRAS*, 501, 5319
- Ball N. M., Brunner R. J., 2012, *International Journal of Modern Physics D*
- Baron D., 2019, Machine Learning in Astronomy: A Practical Overview ([arXiv:1904.07248](https://arxiv.org/abs/1904.07248)), <http://arxiv.org/abs/1904.07248>
- Breiman L., 1996, *Machine Learning*, 24, 123
- Breiman L., 2001, *Machine Learning*, 45, 5
- Breiman L., Friedman J. H., Olshen R. A., Stone C. J., 1984, *Classification and Regression Trees*, 1st edition edn. Chapman and Hall/CRC, Boca Raton, Fla.
- CHIME/FRB Collaboration et al., 2021, *ApJS*, 257, 59
- Caleb M., Stappers B. W., Rajwade K., Flynn C., 2019, *MNRAS*, 484, 5500
- Chaikova A., Kostunin D., Popov S. B., 2022, Model-Independent Classification of Events from the First CHIME/FRB Fast Radio Burst Catalog ([arXiv:2202.10076](https://arxiv.org/abs/2202.10076)), <http://arxiv.org/abs/2202.10076>
- Chawla N. V., Bowyer K. W., Hall L. O., Kegelmeyer W. P., 2002, *Journal of Artificial Intelligence Research*, 16, 321
- Chawla P., et al., 2022, *ApJ*, 927, 35
- Chen T., Guestrin C., 2016, in Proceedings of the 22nd ACM SIGKDD International Conference on Knowledge Discovery and Data Mining. pp 785–794 ([arXiv:1603.02754](https://arxiv.org/abs/1603.02754)), [doi:10.1145/2939672.2939785](https://arxiv.org/abs/1603.02754), <http://arxiv.org/abs/1603.02754>
- Chen B. H., Hashimoto T., Goto T., Kim S. J., Santos D. J. D., On A. Y. L., Lu T.-Y., Hsiao T. Y.-Y., 2021, *MNRAS*
- Connor L., van Leeuwen J., 2018, *AJ*, 156, 256
- Cordes J. M., Chatterjee S., 2019, *ARA&A*, 57, 417
- Cordes J. M., Lazio T. J. W., 2003, NE2001.I. A New Model for the Galactic Distribution of Free Electrons and Its Fluctuations ([arXiv:astro-ph/0207156](https://arxiv.org/abs/astro-ph/0207156)), <http://arxiv.org/abs/astro-ph/0207156>
- Cortes C., Vapnik V., 1995, in *Machine Learning*. pp 273–297
- Cui X.-H., et al., 2022, *Ap&SS*, 367, 66
- Deng W., Zhang B., 2014, *ApJ*, 783, L35
- Dolag K., Gaensler B. M., Beck A. M., Beck M. C., 2015, *MNRAS*, 451, 4277
- Drucker H., 1997, Improving Regressors Using Boosting Techniques
- Ellis G. F. R., 2007, *General Relativity and Gravitation*, 39, 1047
- Etherington I., 1933, *The London, Edinburgh, and Dublin Philosophical Magazine and Journal of Science*, 15, 761
- Farah W., et al., 2019, *MNRAS*, 488, 2989
- Fisher A., Rudin C., Dominici F., 2019, *Journal of Machine Learning Research*, 20, 1
- Fix E., Hodges J. L., 1989, *International Statistical Review / Revue Internationale de Statistique*, 57, 238
- Fonseca E., et al., 2020, *ApJ*, 891, L6
- Freund Y., Schapire R. E., 1997, *Journal of Computer and System Sciences*, 55, 119
- Friedman J., Hastie T., Tibshirani R., 1998, *Annals of Statistics*, 28, 2000
- Fukugita M., Hogan C. J., Peebles P. J. E., 1998, *ApJ*, 503, 518
- Gao H., Li Z., Zhang B., 2014, *ApJ*, 788, 189
- Guo H.-Y., Wei H., 2022, *J. Cosmology Astropart. Phys.*, 2022, 010
- Hashimoto T., et al., 2020, *MNRAS*, 498, 3927
- Hashimoto T., et al., 2022, *MNRAS*, 511, 1961
- Hastie T., Tibshirani R., Friedman J. H., 2009, *The Elements of Statistical Learning: Data Mining, Inference, and Prediction*. 1 Vol. 2, Springer, New York, <http://link.springer.com/book/10.1007/978-0-387-21606-5>
- Hofmann T., Schölkopf B., Smola A. J., 2008, *The Annals of Statistics*, 36, 1171
- Inoue S., 2004, *MNRAS*, 348, 999
- Ioka K., 2003, *ApJ*, 598, L79
- Ivezić Ž., Connolly A. J., VanderPlas J. T., Gray A., 2014, *Statistics, Data Mining, and Machine Learning in Astronomy: A Practical Python Guide for the Analysis of Survey Data*. Princeton University Press, [doi:10.1515/9781400848911](https://doi.org/10.1515/9781400848911), <https://www.degruyter.com/document/doi/10.1515/9781400848911/html>
- Katz J. I., 2016, *Modern Physics Letters A*, 31, 1630013
- Katz J. I., 2022, The Sources of Fast Radio Bursts ([arXiv:2207.13241](https://arxiv.org/abs/2207.13241)), <http://arxiv.org/abs/2207.13241>
- Ke G., Meng Q., Finley T., Wang T., Chen W., Ma W., Ye Q., Liu T.-Y., 2017, in *Advances in Neural Information Processing Systems*. Curran Associates, Inc., <https://proceedings.neurips.cc/paper/2017/hash/6449f44a102fde848669bdd9eb6b76fa-Abstract.html>
- Lemaître G., Nogueira F., Aridas C. K., 2017, *The Journal of Machine Learning Research*, 18, 559
- Li Z., Gao H., Wei J.-J., Yang Y.-P., Zhang B., Zhu Z.-H., 2020, *MNRAS*, 496, L28
- Li D., et al., 2021a, *Nature*, 598, 267
- Li X. J., Dong X. F., Zhang Z. B., Li D., 2021b, *ApJ*, 923, 230
- Loh W.-Y., 2011, *WIREs Data Mining and Knowledge Discovery*, 1, 14
- Loh W.-Y., 2014, *International Statistical Review*, 82, 329
- Lorimer D. R., Bailes M., McLaughlin M. A., Narkevic D. J., Crawford F., 2007, *Science*, 318, 777
- Lu W., Piro A. L., Waxman E., 2020, *MNRAS*, 498, 1973
- Macquart J.-P., et al., 2020, *Nature*, 581, 391
- Marcote B., et al., 2020, *Nature*, 577, 190
- Mayr A., Binder H., Gefeller O., Schmid M., 2014, *Methods of Information in Medicine*, 53, 419
- Palaniswamy D., Li Y., Zhang B., 2018, *ApJ*, 854, L12
- Pedregosa F., et al., 2011, *The Journal of Machine Learning Research*, 12, 2825
- Petroff E., Hessels J. W. T., Lorimer D. R., 2022, *A&ARv*, 30, 2
- Platts E., Weltman A., Walters A., Tendulkar S. P., Gordin J. E. B., Kandhai S., 2019, *Phys. Rep.*, 821, 1
- Pleunis Z., et al., 2021, *ApJ*, 923, 1
- Prochaska J. X., Zheng Y., 2019, *MNRAS*
- Ravi V., 2019, *Nature Astronomy*, 3, 928
- Rybicki G. B., Lightman A. P., 1979, *Radiative processes in astrophysics*. New York, Wiley-Interscience, 1979. 393 p.
- Santos M. S., Soares J. P., Abreu P. H., Araujo H., Santos J., 2018, *IEEE Computational Intelligence Magazine*, 13, 59
- Sasaki Y., 2007, *Teach tutor mater*, 1, 1
- Schapire R. E., Singer Y., 1999, in *Machine Learning*. pp 80–91
- Shannon R. M., et al., 2018, *Nature*, 562, 386
- Spitler L. G., et al., 2016, *Nature*, 531, 202

- Tendulkar S. P., et al., 2017, *ApJ*, 834, L7
 The CHIME/FRB Collaboration 2019, *Nature*, 566, 230
 Thornton D., et al., 2013, *Science*, 341, 53
 Timofeev R., 2004, PhD thesis, Humboldt University, Berlin
 Virtanen P., et al., 2020, *Nature Methods*, 17, 261
 Wagstaff K. L., et al., 2016, *PASP*, 128, 084503
 Wu D., Cao H., Lv N., Fan J., Tan X., Yang S., 2019, *ApJ*, 887, L10
 Xiao D., Dai Z.-G., 2022, *A&A*, 657, L7
 Xiao D., Wang F., Dai Z., 2021, *Science China Physics, Mechanics, and Astronomy*, 64, 249501
 Xiao D., Wang F., Dai Z., 2022, Technical Report arXiv: 2203.14198, Fast Radio Bursts, <http://arxiv.org/abs/2203.14198>. arXiv (arXiv:2203.14198), <http://arxiv.org/abs/2203.14198>
 Xu J., Han J. L., 2015, *Research in Astronomy and Astrophysics*, 15, 1629
 Yamasaki S., Totani T., 2020, *ApJ*, 888, 105
 Yang X., et al., 2021, *MNRAS*
 Zhang B., 2018, *ApJ*, 867, L21
 Zhang B., 2020, *Nature*, 587, 45
 Zhang Y. G., Gajjar V., Foster G., Siemion A., Cordes J., Law C., Wang Y., 2018, *ApJ*, 866, 149
 Zhang R. C., Zhang B., Li Y., Lorimer D. R., 2021, *MNRAS*, 501, 157
 Zhang K., Li L., Zhang Z., Li Q., Luo J., Jiang M., 2022, *Universe*, 8, 355
 Zhong S.-Q., Xie W.-J., Deng C.-M., Li L., Dai Z.-G., Zhang H.-M., 2022, *ApJ*, 926, 206
 Zhou B., Li X., Wang T., Fan Y.-Z., Wei D.-M., 2014, *Phys. Rev. D*, 89, 107303
 van Rijbergen C. J., 1979, Information Retrieval. Butterworth

APPENDIX A: DERIVATION OF BRIGHTNESS TEMPERATURE T_B

In the literature, the derivation of T_B for FRBs has not properly considered the redshift correction (Zhang 2020; Xiao et al. 2021; Xiao & Dai 2022). We suggest that the proper correction is Equation (3). In the following, we present two independent proofs to justify it.

A1 The D_A approach

For an FRB source with specific intensity I_{ν_0} at the cosmic rest-frame frequency ν_0 , the brightness temperature T_B at ν_0 can be defined using the Rayleigh-Jeans approximation of the blackbody law:

$$I_{\nu_0} d\nu_0 = \frac{2\nu_0 k_B T_B}{c^2} d\nu_0, \quad (\text{A1})$$

where k_B is Boltzmann constant.

Suppose the observed specific intensity is I_ν and the observed frequency is $\nu = \nu_0/(1+z)$. Since I_ν/ν^3 should remain constant (Rybicki & Lightman 1979), one can write

$$I_\nu d\nu = \frac{I_{\nu_0} d\nu_0}{(1+z)^4} = \frac{2\nu_0 k_B T_B}{c^2 (1+z)^3} d\nu. \quad (\text{A2})$$

The observed solid angle of the FRB emission region can be written as

$$\Delta\Omega = \frac{\pi R^2}{D_A^2} = \frac{\pi(c\Delta t_0)^2}{D_A^2}, \quad (\text{A3})$$

where R is the radius of the emission region estimated by the

light travel distance in the duration of the FRB, $R = c\Delta t_0$, Δt_0 is the duration of the FRB at the source, and D_A is the angular diameter distance of the FRB.

Finally, the observed specific flux S_ν can be expressed as

$$S_\nu d\nu = \Delta\Omega I_\nu d\nu \quad (\text{A4})$$

Substituting Eq.(A2) to Eq.(A4), one finally obtains

$$\begin{aligned} T_B &= \frac{S_\nu D_A^2}{2\pi k_B (\nu \Delta t)^2} (1+z)^3 \\ &= 1.1 \times 10^{35} \text{ K} \left(\frac{S_\nu}{\text{Jy}} \right) \left(\frac{\nu}{\text{GHz}} \right)^{-2} \left(\frac{\Delta t}{\text{ms}} \right)^{-2} \left(\frac{D_A}{\text{Gpc}} \right)^2 (1+z)^3 \end{aligned} \quad (\text{A5})$$

Where $\Delta t = (1+z)\Delta t_0$ is observed duration, and the $(1+z)$ factors from Δt and ν cancel out. This is one expression in Eq.(3).

A2 The D_L approach

Another route to derive this expression of brightness temperature is similar to the derivation of the Stefan-Boltzmann law. The specific luminosity of the FRB can be expressed as

$$L_{\nu_0} d\nu_0 = 4\pi R^2 \pi I_{\nu_0} d\nu_0. \quad (\text{A6})$$

From the definition of luminosity distance D_L , the observed specific flux S_ν can be written as:

$$S_\nu d\nu = \frac{L_{\nu_0} d\nu_0}{4\pi D_L^2} \quad (\text{A7})$$

Substituting Eq.(A1) to Eq.(A7) and noting $d\nu_0 = (1+z)d\nu$, one finally obtains

$$\begin{aligned} T_B &= \frac{S_\nu D_L^2}{2\pi k_B (\nu \Delta t)^2} \frac{1}{1+z} \\ &= 1.1 \times 10^{35} \text{ K} \left(\frac{S_\nu}{\text{Jy}} \right) \left(\frac{\nu}{\text{GHz}} \right)^{-2} \left(\frac{\Delta t}{\text{ms}} \right)^{-2} \left(\frac{D_L}{\text{Gpc}} \right)^2 \frac{1}{1+z}. \end{aligned} \quad (\text{A8})$$

This is another expression in Eq.(3). Since the two distances are connected through $D_L = D_A(1+z)^2$ for a flat universe, the two expressions are equivalent and the two derivations are consistent with each other.

This paper has been typeset from a $\text{\TeX}/\text{\LaTeX}$ file prepared by the author.